PAPER • OPEN ACCESS

Active locking and entanglement in type II optical parametric oscillators

New Journal of Physics
The open access journal at the forefront of physics

Deutsche Physikalische Gesellschaft DPG
IOP Institute of Physics

Published in partnership with: Deutsche Physikalische Gesellschaft and the Institute of Physics

OPEN ACCESS

RECEIVED
6 August 2017

REVISED
23 November 2017

ACCEPTED FOR PUBLICATION
21 December 2017

PUBLISHED
5 February 2018

PAPER

Active locking and entanglement in type II optical parametric oscillators

Joaquín Ruiz-Rivas[1], **Germán J de Valcárcel**[1] **and Carlos Navarrete-Benlloch**[2,3,4]

[1] Departament d'Òptica, Universitat de València, Dr. Moliner 50, E-46100 Burjassot, Spain
[2] Max-Planck-Institute für die Physik des Lichts, Staudtstr. 2, D-91058 Erlangen, Germany
[3] Institute for Theoretical Physics, Universität Erlangen-Nürnberg, Staudtstr. 7, D-91058 Erlangen, Germany
[4] Max-Planck-Institut für Quantenoptik, Hans-Kopfermann-str. 1, D-85748 Garching, Germany

E-mail: derekkorg@gmail.com

Keywords: nonlinear optics, quantum optics, optical parametric oscillators, quantum fluctuations

Abstract

Type II optical parametric oscillators are amongst the highest-quality sources of quantum-correlated light. In particular, when pumped above threshold, such devices generate a pair of bright orthogonally-polarized beams with strong continuous-variable entanglement. However, these sources are of limited practical use, because the entangled beams emerge with different frequencies and a diffusing phase difference. It has been proven that the use of an internal wave-plate coupling the modes with orthogonal polarization is capable of locking the frequencies of the emerging beams to half the pump frequency, as well as reducing the phase-difference diffusion, at the expense of reducing the entanglement levels. In this work we characterize theoretically an alternative locking mechanism: the injection of a laser at half the pump frequency. Apart from being less invasive, this method should allow for an easier real-time experimental control. We show that such an injection is capable of generating the desired phase locking between the emerging beams, while still allowing for large levels of entanglement. Moreover, we find an additional region of the parameter space (at relatively large injections) where a mode with well defined polarization is in a highly amplitude-squeezed state.

1. Introduction

Optical parametric oscillators (OPOs) are optical cavities containing a crystal with second order nonlinearity. When pumped with a laser at frequency $2\omega_0$, these are able to generate beams at frequecies ω_s (signal) and ω_i (idler) such that $\omega_s + \omega_i = 2\omega_0$, through the nonlinear process known as parametric down conversion [1, 2]. Classically, the generation of the down-converted field requires the nonlinear gain to compensate for the cavity losses, what means that the OPO has to be pumped above a certain threshold power in order for signal and idler to start oscillating inside the cavity [1, 2]. Quantum mechanically, on the other hand, down-converted pairs are generated even below the classical threshold, what confers the signal and idler fields with very interesting quantum correlations [3].

In particular, type I OPOs, in which both signal and idler are linearly polarized along the same direction, hold the record for quadrature noise reduction or single-mode squeezing (97% below vacuum fluctuations in [4], see also [5–9] for previous experiments achieving more than 90% of noise reduction); this is manifested in the mode at the degenerate frequency $\omega_s = \omega_i = \omega_0$, but squeezing is large only when working close to threshold [10]. As for the applications of this quantum-correlated light source, on one hand, squeezed light is a basic resource in the field of high-precission measurements, helping overcome the standard quantum limit imposed by vacuum fluctuations [11–14]. On the other hand, mixing the output of two single-mode squeezers on a beam splitter, one can obtain a pair of entangled beams (in the continuous-variable, Einstein–Podolsky–Rosen sense [15]), what makes these devices a basic resource also for continuous-variable quantum information protocols [16–18]; however, this method for the generation of entanglement requires the nonlinear cavities to be

precisely locked to generate indistinguishable down-converted fields whose squeezing occurs in two orthogonal quadratures, which introduces one level of complexity.

Of more interest for our current work are type II OPOs, that is, OPOs in which signal and idler have orthogonal polarizations (one following the extraordinary crystal axis, and the other one the ordinary), making the down conversion intrinsically nondegenerate [1, 2]. Just as the degenerate OPO, there is an observable which shows large squeezing levels only close to threshold, which in this case corresponds to the sum of the phases of signal and idler; in other words, close to threshold, type II OPOs show signal-idler phase anticorrelations beyond the standard quantum limit [19–21]. But nondegenerate OPOs have one more interesting property: they are invariant under changes of the signal-idler phase difference, what means that quantum noise is able to act on this variable without bounds, making it diffuse and eventually completely undetermined (in the quantum mechanical sense) [2, 19, 22–25]. But, invoking now the Heisenberg principle, a completely undetermined phase difference between signal and idler allows for complete noise reduction in their intensisty difference (its canonically conjugate variable); indeed, signal and idler become twin beams above threshold, that is, their amplitudes are perfectly correlated [22, 26, 27]. Hence, nondegenerate OPOs show (ideally) perfect amplitude correlations at any pumping level above threshold, and large phase anti-correlations close to threshold, which means that close to this point they should be in a high-quality continuous-variable entangled state [2, 20, 21, 23]. From a quantum optics perspective, this means that below threshold OPOs should emit a two-mode squeezed vacuum state, while above threshold OPOs would emit a displaced one (a 'bright' EPR state).

However, there are two issues that make above-threshold type II OPOs not practical as EPR sources, specially from a detection point of view. First, the phase-matching conditions ensuring that it is the frequency degenerate process the one with larger gain (lowest threshold) are quite critical, and hence, signal and idler will have different frequencies in general; for example, in the case of [28], where the authors are able to make the frequency difference between signal and idler as small as 150 kHz for a cavity with 8 GHz free spectral range and 6 MHz linewidth, variations of the cavity length on the order of the nanometer can make the oscillation frequencies jump to frequencies separated by several times the free spectral range (mode hopping); second, the signal-idler phase difference is chosen at random at any realization and diffuses with time (rather fast close to threshold), making it virtually impossible to capture the squeezed quadratures in a balanced homodyne detection scheme. Hence, additional signal-idler phase locking techniques are required.

The pioneering example of such locking techniques was introduced in [29–31]. Their idea consisted in embedding in the cavity a $\lambda/4$ plate with its fast axis misaligned with respect to the extraordinary axis of the nonlinear crystal. The plate introduces a coupling between the signal and idler modes which breaks the phase invariance of the OPO, and it was then shown in [29] that in a given region of the parameter space (in particular of the detunings) the frequencies of signal and idler get locked to ω_0; this OPO is known as the *self-phase-locked OPO*, and was already demonstrated experimentally in [31]. Note that, as mentioned, this self-locking effect is accomplished by breaking the phase symmetry of the OPO, and hence, one should expect a degradation of the signal-idler intensity correlations, or, equivalently, of the noncritical squeezing induced by spontaneous polarization symmetry breaking described in [32]. For example, in [31] the intensity-difference fluctuations showed 89% quantum noise reduction prior to the introduction of the plate, while after obtaining frequency degeneracy through the self-phase-locking mechanism this value fell down to a more humble 65%.

In the present article we study an alternative locking mechanism which consists in the injection of a laser signal at frequency degeneracy ω_0, what is less invasive and more controllable at real time than the introduction of a $\lambda/4$ wave plate; we will call *actively-phase-locked OPO* to such OPO configuration. We show how locking of the signal and idler frequencies to the subharmonic ω_0 can be achieved, while still obtaining large entanglement levels. This locking technique is reminiscent of our previous work in frequency-degenerate type I OPOs tuned to the first family of transverse modes [2, 24, 25, 33–35], in which we proposed injecting a TEM_{10} mode at the subharmonic to lock the phase difference between the down-converted modes with opposite orbital angular momentum [34].

The article is organized as follows. In the next section we introduce our OPO model, providing the set of stochastic equations within the positive P representation which will allow us to study both its classical and quantum dynamics in detail. Particularizing to a configuration that we will denote by 'symmetric', next we find the classical phase diagram of the system analytically, showing the regimes where frequency locking is expected to appear. Still within this symmetric configuration, we then provide analytical expressions for the quantum correlations of the system, putting special emphasis on the level of signal-idler entanglement at the locking points. In the section before the conclusions, we move out of the symmetric configuration, which is quite challenging to achieve in real experiments, and perform a numerical study that proves all the analytic conclusions of the symmetric case to hold also in this case.

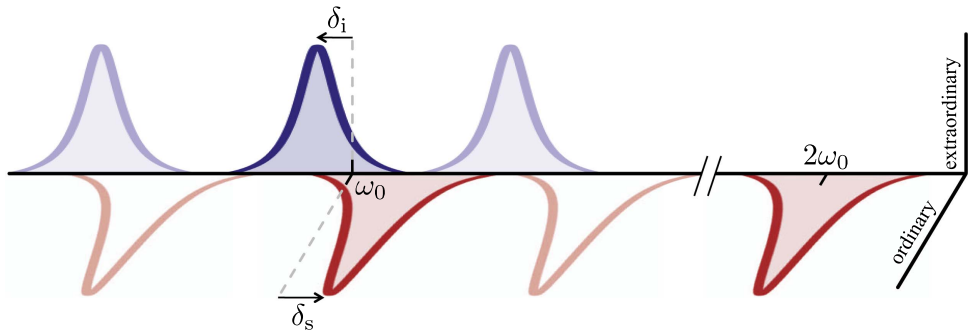

Figure 1. Resonance scheme of the type II OPO considered in this work. The birefringence of the crystal breaks the degeneracy between the modes with ordinary and extraordinary polarization, which experience different refractive indices (here, for definiteness, we assume larger index along the extraordinary axis, the so-called positive uniaxial crystals [1]). We show the pump resonance at frequency $2\omega_0$, and three resonances around the subharmonic ω_0, two of which overlap at that frequency and correspond to the signal and idler down-converted modes.

2. Model for the actively-phase-locked OPO

We consider an optical cavity with a thin $\chi^{(2)}$ nonlinear crystal at its center ($z = 0$), where the electric field operator at the relevant frequencies can be approximately written as [2]

$$\hat{\mathbf{E}}_j(\mathbf{r}_\perp, t) = \mathrm{i}E_j\boldsymbol{\varepsilon}_j \mathrm{e}^{-r^2/w_j^2}\hat{a}_j \mathrm{e}^{-\mathrm{i}\omega_j t} + \mathrm{H.c.}. \tag{1}$$

The index j takes the values 'p', 's' and 'i' for pump, signal, and idler, respectively ($\omega_s = \omega_i = \omega_0 = \omega_p/2$). The single-photon field amplitudes are $E_j = \sqrt{\hbar\omega_j/\pi\varepsilon_0 n_j L_j w_j^2}$ for a ring cavity, where n_j, L_j, w_j, and $\boldsymbol{\varepsilon}_j$ are, respectively, crystal's refractive index, optical cavity length, transverse spot size at the cavity waist, and polarization of the corresponding mode. For a Fabry–Perot cavity the single-photon field amplitudes have an extra $\sqrt{2}$ factor. $\mathbf{r}_\perp = (x, y)$ is the transverse coordinate vector, with $r = |\mathbf{r}_\perp|$, and we have assumed there are TEM_{00} transverse modes resonating at the three relevant frequencies, giving rise to the simple Gaussian transverse profile of the expression. We work in a picture rotating at frequency $2\omega_0$ for the pump, and ω_0 for signal and idler. The annihilation ($\hat{a}_j$) and creation ($\hat{a}_j^\dagger$) operators satisfy canonical commutation relations $[\hat{a}_j, \hat{a}_l^\dagger] = \delta_{jl}$.

The resonance scheme and polarization of the fields are sketched in figure 1: the pump is polarized along the ordinary axis of the crystal and resonates at frequency $2\omega_0$, while, by convention, signal and idler are polarized within the ordinary and extraordinary axis, respectively, and resonate at frequencies $\omega_0 + \delta_{s,i}$, with $|\delta_{s,i}|$ smaller or on the order of their cavity linewidth $\gamma_s = \gamma_i$, taken equal for signal and idler for simplicity. Apart from pumping the cavity with a laser at frequency $2\omega_0$ with ordinary polarization, we inject an external laser field (in phase with the pump drive) at the degenerate frequency ω_0 with polarization $\boldsymbol{\varepsilon}_0 = \mathrm{e}^{-\mathrm{i}\theta_0}\mathbf{e}_o \cos\varphi_0 + \mathrm{e}^{\mathrm{i}\theta_0}\mathbf{e}_e \sin\varphi_0$, where $\mathbf{e}_o$ and $\mathbf{e}_e$ are unit vectors following, respectively, the ordinary and extraordinary axes of the crystal. Including cavity losses through the usual Lindblad terms, the master equation governing the evolution of the state of the system reads [2, 36, 37]

$$\frac{\mathrm{d}\hat{\rho}}{\mathrm{d}t} = \frac{1}{\mathrm{i}\hbar}[\hat{H}, \hat{\rho}] + \sum_{j=\mathrm{p,s,i}} \gamma_j(2\hat{a}_j\hat{\rho}\hat{a}_j^\dagger - \hat{a}_j^\dagger\hat{a}_j\hat{\rho} - \hat{\rho}\hat{a}_j^\dagger\hat{a}_j), \tag{2}$$

in the aforementioned rotating picture where the Hamiltonian can be written as $\hat{H} = \hat{H}_0 + \hat{H}_{\mathrm{PDC}} + \hat{H}_{\mathrm{inj}}$, with

$$\hat{H}_0 = \hbar\delta_s\hat{a}_s^\dagger\hat{a}_s + \hbar\delta_i\hat{a}_i^\dagger\hat{a}_i, \tag{3a}$$

$$\hat{H}_{\mathrm{PDC}} = \mathrm{i}\hbar\chi(\hat{a}_p\hat{a}_s^\dagger\hat{a}_i^\dagger - \hat{a}_p^\dagger\hat{a}_s\hat{a}_i), \tag{3b}$$

$$\hat{H}_{\mathrm{inj}} = \sum_{j=\mathrm{p,s,i}} \mathrm{i}\hbar\,(\mathcal{E}_j\hat{a}_j^\dagger - \mathcal{E}_j^*\hat{a}_j). \tag{3c}$$

In this expression, the down-conversion rate χ is proportional to the crystal's nonlinear susceptibility, and the damping rates are related to the (intensity) transmisivities of the mirror at the corresponding frequency, $\mathcal{T}_j$, by $\gamma_j \approx c\mathcal{T}_j/4L_j$ for Fabry–Perot cavities and $\gamma_j \approx c\mathcal{T}_j/2L_j$ for ring cavities. In addition, the injection parameters can be approximately written in terms of the power P_j of the injected lasers at frequencies $2\omega_0$ and ω_0 as $\mathcal{E}_p = \sqrt{\gamma_p P_{2\omega_0}/\hbar\omega_0}$, $\mathcal{E}_s = \sqrt{2\gamma_s P_{\omega_0}/\hbar\omega_0}\,\mathrm{e}^{-\mathrm{i}\theta_0}\cos\varphi_0$, and $\mathcal{E}_i = \sqrt{2\gamma_s P_{\omega_0}/\hbar\omega_0}\,\mathrm{e}^{\mathrm{i}\theta_0}\sin\varphi_0$, where we have taken the phase of the driving lasers as a reference.

In order to get analytical insight, and following previous works [24, 25, 34, 35], we map this master equation into a set of stochastic Langevin equations by using the positive P phase-space representation [38]. This is a procedure by which an independent complex stochastic variable is associated to each bosonic operator, that is, $\{\alpha_j,\ \alpha_j^+\}_{j=\mathrm{p,s,i}}$ to $\{\hat{a}_j,\ \hat{a}_j^\dagger\}_{j=\mathrm{p,s,i}}$. Quantum expectation values of any operator are then obtained as stochastic averages by replacing the bosonic operators by their corresponding stochastic variable in the normally-ordered version of the operator. In contrast to phase-space methods (such as the Wigner representation) that do not require enlarging the phase space of the bosonic modes, the positive P representation allows for an exact mapping between the master equation and a set of stochastic equations with a minimal extension of the phase space (it only doubles it). In particular, it is not difficult to show [2] that the stochastic Langevin equations associated with the master equation (2) read (the overdot denotes derivative with respect to time)

$$\dot{\alpha}_\mathrm{p} = \mathcal{E}_\mathrm{p} - \gamma_\mathrm{p}\alpha_\mathrm{p} - \chi\alpha_\mathrm{s}\alpha_\mathrm{i}, \tag{4a}$$

$$\dot{\alpha}_\mathrm{p}^+ = \mathcal{E}_\mathrm{p} - \gamma_\mathrm{p}\alpha_\mathrm{p}^+ - \chi\alpha_\mathrm{s}^+\alpha_\mathrm{i}^+, \tag{4b}$$

$$\dot{\alpha}_\mathrm{s} = \mathcal{E}_\mathrm{s} - (\gamma_\mathrm{s} + \mathrm{i}\delta_\mathrm{s})\alpha_\mathrm{s} + \chi\alpha_\mathrm{p}\alpha_\mathrm{i}^+ + \sqrt{\chi\alpha_\mathrm{p}}\,\xi(t), \tag{4c}$$

$$\dot{\alpha}_\mathrm{s}^+ = \mathcal{E}_\mathrm{s} - (\gamma_\mathrm{s} - \mathrm{i}\delta_\mathrm{s})\alpha_\mathrm{s}^+ + \chi\alpha_\mathrm{p}^+\alpha_\mathrm{i} + \sqrt{\chi\alpha_\mathrm{p}^+}\,\xi^+(t), \tag{4d}$$

$$\dot{\alpha}_\mathrm{i} = \mathcal{E}_\mathrm{i} - (\gamma_\mathrm{s} + \mathrm{i}\delta_\mathrm{i})\alpha_\mathrm{i} + \chi\alpha_\mathrm{p}\alpha_\mathrm{s}^+ + \sqrt{\chi\alpha_\mathrm{p}}\,\xi^*(t), \tag{4e}$$

$$\dot{\alpha}_\mathrm{i}^+ = \mathcal{E}_\mathrm{i} - (\gamma_\mathrm{s} - \mathrm{i}\delta_\mathrm{i})\alpha_\mathrm{i}^+ + \chi\alpha_\mathrm{p}^+\alpha_\mathrm{s} + \sqrt{\chi\alpha_\mathrm{p}^+}\,\xi^{+*}(t), \tag{4f}$$

where we have defined independent complex Gaussian noises $\xi(t)$ and $\xi^+(t)$, with zero mean, and only non-zero two-time correlators

$$\langle\xi(t)\xi^*(t')\rangle = \langle\xi^+(t)\xi^{+*}(t')\rangle = \delta(t-t'). \tag{5}$$

In order to reduce the number of parameters of the problem, we now make some variable changes; in particular, we redefine time as $\tau = \gamma_\mathrm{s}t$, the coherent amplitudes as

$$\beta_\mathrm{p} = \frac{\chi}{\gamma_\mathrm{s}}\alpha_\mathrm{p}, \qquad \beta_\mathrm{s,i} = \frac{\chi}{\sqrt{\gamma_\mathrm{s}\gamma_\mathrm{p}}}\alpha_\mathrm{s,i}\exp(\pm\mathrm{i}\theta_0) \tag{6}$$

and the noises as

$$\eta(\tau) = \frac{\mathrm{e}^{\mathrm{i}\theta_0}}{\sqrt{\gamma_\mathrm{s}}}\xi(t), \qquad \eta^+(\tau) = \frac{\mathrm{e}^{-\mathrm{i}\theta_0}}{\sqrt{\gamma_\mathrm{s}}}\xi^+(t), \tag{7}$$

which satisfy the statistical properties (5), but now with respect to the dimensionless time τ. In terms of these new variables, the Langevin equations read

$$\dot{\beta}_\mathrm{p} = \kappa(\sigma - \beta_\mathrm{p} - \beta_\mathrm{s}\beta_\mathrm{i}), \tag{8a}$$

$$\dot{\beta}_\mathrm{p}^+ = \kappa(\sigma - \beta_\mathrm{p}^+ - \beta_\mathrm{s}^+\beta_\mathrm{i}^+), \tag{8b}$$

$$\dot{\beta}_\mathrm{s} = \varepsilon_\mathrm{s} - (1 + \mathrm{i}\Delta_\mathrm{s})\beta_\mathrm{s} + \beta_\mathrm{p}\beta_\mathrm{i}^+ + g\sqrt{\beta_\mathrm{p}}\,\eta(\tau), \tag{8c}$$

$$\dot{\beta}_\mathrm{s}^+ = \varepsilon_\mathrm{s} - (1 - \mathrm{i}\Delta_\mathrm{s})\beta_\mathrm{s}^+ + \beta_\mathrm{p}^+\beta_\mathrm{i} + g\sqrt{\beta_\mathrm{p}^+}\,\eta^+(\tau), \tag{8d}$$

$$\dot{\beta}_\mathrm{i} = \varepsilon_\mathrm{i} - (1 + \mathrm{i}\Delta_\mathrm{i})\beta_\mathrm{i} + \beta_\mathrm{p}\beta_\mathrm{s}^+ + g\sqrt{\beta_\mathrm{p}}\,\eta^*(\tau), \tag{8e}$$

$$\dot{\beta}_\mathrm{i} = \varepsilon_\mathrm{i} - (1 - \mathrm{i}\Delta_\mathrm{i})\beta_\mathrm{i}^+ + \beta_\mathrm{p}^+\beta_\mathrm{s} + g\sqrt{\beta_\mathrm{p}^+}\,\eta^{+*}(\tau), \tag{8f}$$

where we have defined the parameters

$$\kappa = \frac{\gamma_\mathrm{p}}{\gamma_\mathrm{s}}, \qquad \sigma = \frac{\chi\mathcal{E}_\mathrm{p}}{\gamma_\mathrm{s}\gamma_\mathrm{p}}, \ \Delta_j = \frac{\delta_j}{\gamma_\mathrm{s}}, \ \varepsilon_\mathrm{s,i} = \frac{g}{\gamma_\mathrm{s}}|\mathcal{E}_\mathrm{s,i}|, \qquad g = \frac{\chi}{\sqrt{\gamma_\mathrm{s}\gamma_\mathrm{p}}}. \tag{9}$$

Note that this Langevin system is independent of θ_0, and hence, the physics is only sensitive to the parameter φ_0 of the injection's polarization.

In order to get some analytic insight, in the rest of the article (with the exception of the last section) we are going to simplify the problem to what we will call *symmetric configuration* of the actively-phase-locked OPO: we assume the detunings to be opposite, that is, $\Delta_\mathrm{s} = -\Delta_\mathrm{i} = \Delta > 0$, and inject with $\varphi_0 = \pi/4$ (arbitrary polarization ellipse along the $\pm 45^\circ$ axis), so that signal and idler get equally pumped, $\varepsilon_\mathrm{s} = \varepsilon_\mathrm{i} \equiv \sqrt{\mathcal{P}}$. Furthermore, we consider the $\kappa \gg 1$ limit in which the pump can be adiabatically eliminated ($\dot{\beta}_\mathrm{p} = \dot{\beta}_\mathrm{p}^+ = 0$ in the previous equations). Taking all these considerations into account, we can reduce our model equation (8) to

$$\dot{\beta}_\mathrm{s} = \sqrt{\mathcal{P}} - (1 + \mathrm{i}\Delta)\beta_\mathrm{s} + \tilde{\beta}_\mathrm{p}\beta_\mathrm{i}^+ + g\sqrt{\tilde{\beta}_\mathrm{p}}\,\eta(\tau), \tag{10a}$$

$$\dot{\beta}_{\rm s}^{+} = \sqrt{\mathcal{P}} - (1 - {\rm i}\Delta)\beta_{\rm s}^{+} + \tilde{\beta}_{\rm p}^{+}\beta_{\rm i} + g\sqrt{\tilde{\beta}_{\rm p}^{+}}\,\eta^{+}(\tau), \tag{10b}$$

$$\dot{\beta}_{\rm i} = \sqrt{\mathcal{P}} - (1 - {\rm i}\Delta)\beta_{\rm i} + \tilde{\beta}_{\rm p}\beta_{\rm s}^{+} + g\sqrt{\tilde{\beta}_{\rm p}}\,\eta^{*}(\tau), \tag{10c}$$

$$\dot{\beta}_{\rm i}^{+} = \sqrt{\mathcal{P}} - (1 + {\rm i}\Delta)\beta_{\rm i}^{+} + \tilde{\beta}_{\rm p}^{+}\beta_{\rm s} + g\sqrt{\tilde{\beta}_{\rm p}^{+}}\,\eta^{+*}(\tau), \tag{10d}$$

with $\tilde{\beta}_{\rm p} = \sigma - \beta_{\rm s}\beta_{\rm i}$ and $\tilde{\beta}_{\rm p}^{+} = \sigma - \beta_{\rm s}^{+}\beta_{\rm i}^{+}$.

These are the final equations that will model quantum mechanically our system in the remaining of the paper. In this work we are interested in the quantum properties of the down-converted field. In particular, defining a polarization mode

$$\varepsilon_{\theta} = [{\rm e}^{-{\rm i}(\theta_0-\theta)}\mathbf{e}_{\rm e} + {\rm e}^{{\rm i}(\theta_0-\theta)}\mathbf{e}_{\rm o}]/\sqrt{2}, \tag{11}$$

where we include in the definition the phase θ_0 of the injection beam for later convenience, with associated annihilation operator

$$\hat{a}_{\theta} = [{\rm e}^{{\rm i}(\theta_0-\theta)}\hat{a}_{\rm s} + {\rm e}^{-{\rm i}(\theta_0-\theta)}\hat{a}_{\rm i}]/\sqrt{2}, \tag{12}$$

we will be interested in the noise spectrum associated to one of its quadratures

$$\hat{X}_{\theta}^{\psi} = {\rm e}^{-{\rm i}\psi}\hat{a}_{\theta} + {\rm e}^{{\rm i}\psi}\hat{a}_{\theta}^{\dagger}, \tag{13}$$

which can be obtained as [2]

$$V^{\rm out}(\hat{X}_{\theta}^{\psi};\,\Omega) = 1 + \frac{2}{g^2}\lim_{\tau\to\infty}\int_{-\infty}^{+\infty} {\rm d}\tau'\,\langle\delta x_{\theta}^{\psi}(\tau)\delta x_{\theta}^{\psi}(\tau+\tau')\rangle\,{\rm e}^{-\,{\rm i}\Omega\tau'}, \tag{14}$$

where Ω is the so-called noise frequency (normalized to $\gamma_{\rm s}$), and $x_{\theta}^{\psi} = {\rm e}^{-{\rm i}\psi}\beta_{\theta} + {\rm e}^{{\rm i}\psi}\beta_{\theta}^{+}$ is the stochastic variable accounting for the quadrature associated to the normalized stochastic amplitudes

$$\beta_{\theta} = ({\rm e}^{-{\rm i}\theta}\beta_{\rm s} + {\rm e}^{{\rm i}\theta}\beta_{\rm i})/\sqrt{2}, \tag{15a}$$

$$\beta_{\theta}^{+} = ({\rm e}^{{\rm i}\theta}\beta_{\rm s}^{+} + {\rm e}^{-{\rm i}\theta}\beta_{\rm i}^{+})/\sqrt{2}. \tag{15b}$$

We have also introduced the notation $\delta x_{\theta}^{\psi} = x_{\theta}^{\psi} - \langle x_{\theta}^{\psi}\rangle$. This noise spectrum is the quantity usually measured in a homodyne detection of the field coming out of the cavity when the local oscillator matches the spatio-temporal profile of the down-converted field, and has polarization ε_{θ} and phase ψ relative to the pump. Quantum correlations are manifest whenever $V(\hat{X}_{\theta}^{\psi};\,\Omega) < 1$ for some value of the parameters, in which case we say that quadrature $\hat{X}_{\theta}^{\psi}$ is squeezed at noise frequency Ω. Let us finally remark that in the following we will use the common short-hand notations

$$\hat{Y}_{\theta}^{\psi} = \hat{X}_{\theta}^{\psi+\pi/2},\ \hat{X}_{\theta} = \hat{X}_{\theta}^{\psi=0},\ \hat{Y}_{\theta} = \hat{Y}_{\theta}^{\psi=0} \tag{16}$$

and similarly for the normalized stochastic quadratures

$$y_{\theta}^{\psi} = x_{\theta}^{\psi+\pi/2},\ x_{\theta} = x_{\theta}^{\psi=0},\ y_{\theta} = y_{\theta}^{\psi=0}. \tag{17}$$

3. Classical behavior: frequency locking

Let us first analyze the classical behavior of the system, which will allow us to see the regions of the parameter space where the signal and idler oscillation frequencies get locked. The classical limit can be retrieved by making a coherent-state ansatz for all fields, whose amplitude plays the role of the (normalized) amplitude of the classical electromagnetic fields. Within the positive *P* representation, this is equivalent to replacing the 'plus' amplitudes by the corresponding complex-conjugate ones and setting the noises to zero, leading to

$$\dot{\beta}_{\rm s} = \sqrt{\mathcal{P}} - (1 + {\rm i}\Delta)\beta_{\rm s} + (\sigma - \beta_{\rm s}\beta_{\rm i})\beta_{\rm i}^{*}, \tag{18a}$$

$$\dot{\beta}_{\rm i} = \sqrt{\mathcal{P}} - (1 - {\rm i}\Delta)\beta_{\rm i} + (\sigma - \beta_{\rm s}\beta_{\rm i})\beta_{\rm s}^{*}. \tag{18b}$$

From the expression in equation (1), it is clear that oscillation frequency of the classical fields will be locked to the injection frequency ω_0 whenever this nonlinear system has a stationary solution. On the other hand, the symmetry $\{\beta_{\rm s} \to \beta_{\rm i}^{*},\ \beta_{\rm i} \to \beta_{\rm s}^{*}\}$ of these equations suggests looking for stationary solutions of the type

$$\bar{\beta}_{\rm s} = \bar{\beta}_{\rm i}^{*} = \sqrt{I}\,\exp({\rm i}\varphi). \tag{19}$$

In the remaining of this section we study the conditions under which this type of solutions exist and are stable.

First, it is straightforward to show from (18) that the intensity I of this *symmetric solution* satisfies the third order polynomial

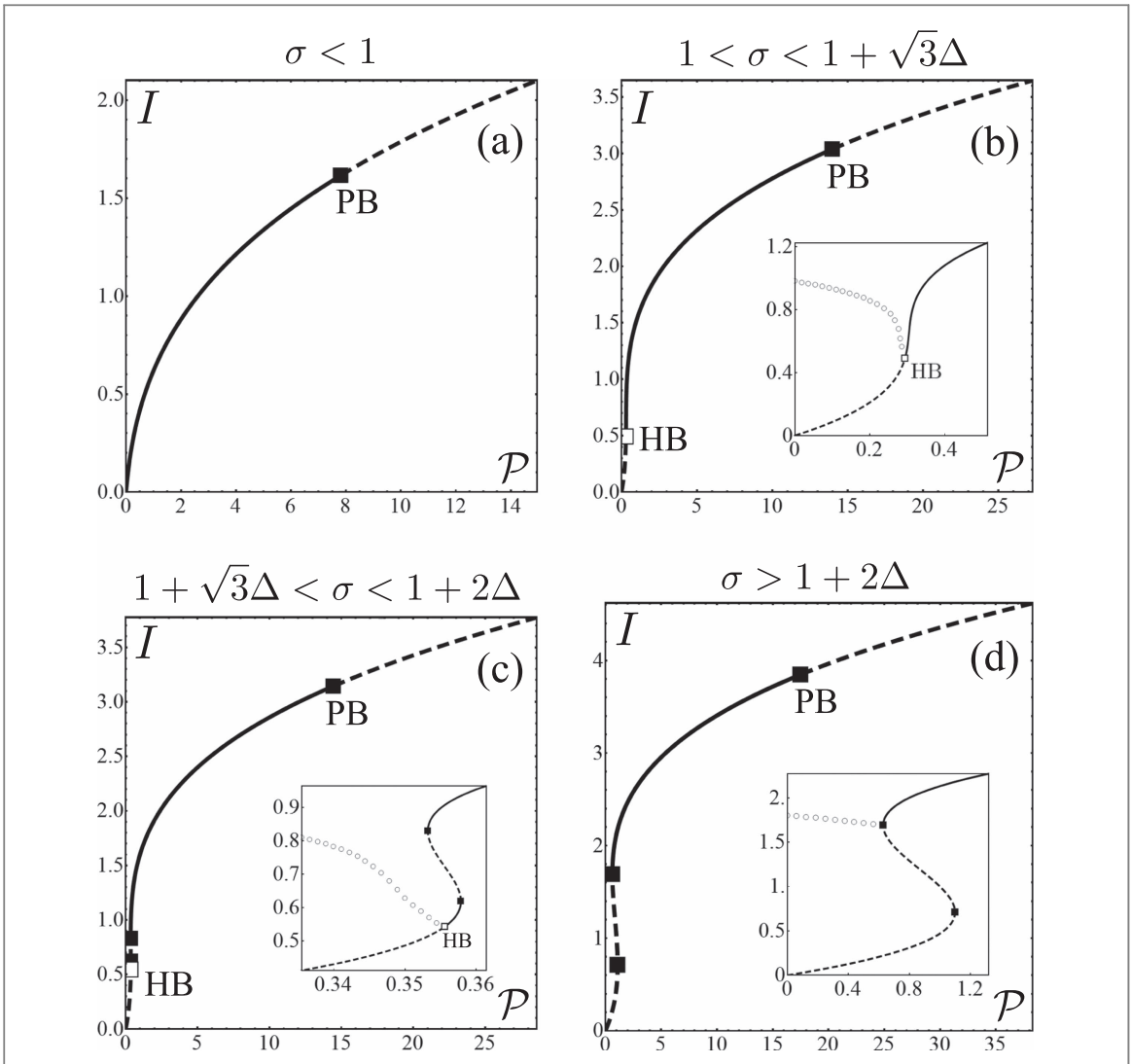

Figure 2. Bifurcation diagrams of the system. The value $\Delta = 0.6$ is chosen for all the figures (the same behavior is found for any other choice), while we set σ to 0.5 in (a), 1.98 in (b), 2.09 in (c), and 2.8 in (d). The black lines correspond to the intensity I of the stationary symmetric solution (19), their solid or dashed character meaning that this solution is stable or unstable, respectively. As explained in the text, for $\sigma > 1$ it is possible to find periodic solutions connecting the $\mathcal{P} = 0$ axis with the stationary branch (at the Hopf bifurcation, marked as HB, for $\sigma < 1 + 2\Delta$ or the upper turning point otherwise). We have checked numerically that these periodic orbits exist, and moreover they are 'symmetric', that is, $\beta_s(\tau) = \beta_i^*(\tau)$. The gray circles correspond in this case to the mean value of $|\beta_s(\tau)|^2$ (half the sum between its maximum and its minimum of oscillation). On the other hand, for relatively large injections there is always a Pitchfork bifurcation in which the symmetric stationary solution becomes unstable in favor of another stationary but asymmetric solution. The insets show simply a zoom of the main figures at low injections.

$$\mathcal{P} = [(I + 1 - \sigma)^2 + \Delta^2]I, \tag{20}$$

with its phase φ uniquely determined from I as $\varphi = \arg\{I + 1 - \sigma - i\Delta\}$. Depending on the parameters, this polynomial can have one or three positive definite solutions (see figure 2); by solving the equation $\partial\mathcal{P}/\partial I = 0$, it is simple to show that the turning points $I_\pm$ have the expression

$$I_\pm = \frac{2}{3}(\sigma - 1) \pm \frac{1}{3}\sqrt{(\sigma - 1)^2 - 3\Delta^2} \tag{21}$$

and hence, they exist only for $\sigma > 1 + \sqrt{3}\,\Delta$. For $\sigma \leqslant 1 + \sqrt{3}\,\Delta$ the solution is therefore single valued.

In order to analyze the stability of this symmetric solution, we will change to a new polarization basis

$$\varepsilon_b = \varepsilon_\varphi \text{ and } \varepsilon_d = \varepsilon_{\varphi - \pi/2}, \tag{22}$$

where ε_b corresponds to the polarization mode excited by the symmetric solution (19) and ε_d to its orthogonal, that is, to what we will call the *bright* and *dark* modes of the system, as we did in previous works [2, 24, 25, 32–35]. In terms of the signal and idler modes, the corresponding normalized amplitudes are given by $\beta_b = (e^{-i\varphi}\beta_s + e^{i\varphi}\beta_i)/\sqrt{2}$ and $\beta_d = i(e^{-i\varphi}\beta_s - e^{i\varphi}\beta_i)/\sqrt{2}$, and satisfy the evolution equations

$$\dot{\beta}_{\rm b} = \sqrt{2\mathcal{P}}\cos\varphi - \beta_{\rm b} - \Delta\beta_{\rm d} + \left(\sigma - \frac{\beta_{\rm b}^2}{2} - \frac{\beta_{\rm d}^2}{2}\right)\beta_{\rm b}^*, \tag{23a}$$

$$\dot{\beta}_{\rm d} = \sqrt{2\mathcal{P}}\sin\varphi - \beta_{\rm d} + \Delta\beta_{\rm b} + \left(\sigma - \frac{\beta_{\rm b}^2}{2} - \frac{\beta_{\rm d}^2}{2}\right)\beta_{\rm d}^*. \tag{23b}$$

In this new basis the symmetric solution (19) $\bar{\beta}_{\rm s,i} = \sqrt{I}\exp(\pm{\rm i}\varphi)$ simply reads $\{\bar{\beta}_{\rm b} = \sqrt{2I}, \bar{\beta}_{\rm d} = 0\}$ and its associated stability matrix is

$$\mathcal{L} = \begin{bmatrix} -1-2I & \sigma - I & -\Delta & 0 \\ \sigma - I & -1-2I & 0 & -\Delta \\ \Delta & 0 & -1 & \sigma - I \\ 0 & \Delta & \sigma - I & -1 \end{bmatrix}. \tag{24}$$

The characteristic polynomial of this stability matrix can be factorized into two second-order polynomials, namely $P_{\rm I}(\lambda) = (\lambda + 1 + \sigma)^2 + \Delta^2 - I^2$ and $P_{\rm II}(\lambda) = (\lambda + 1 - \sigma + 2I)^2 + \Delta^2 - I^2$. The bifurcation diagrams for the different parameter regions are shown in figure 2; now we discuss them in length.

Let us start by studying the instabilities predicted by the first polynomial, whose roots are given by

$$\lambda_{\pm}^{\rm I} = -(1+\sigma) \pm \sqrt{I^2 - \Delta^2}. \tag{25}$$

The condition $\mathrm{Re}\{\lambda_{\pm}^{\rm I}\} = 0$ can only be satisfied for

$$I = \sqrt{(1+\sigma)^2 + \Delta^2} \equiv I_{\rm PB}. \tag{26}$$

The fact that the instability appears without imaginary part in $\lambda_{\pm}^{\rm I}$, and it is located in the upper branch of the S-shaped curve ($I_{\rm PB} > I_+$ for any value of the parameters), signals that it corresponds to a pitchfork or static bifurcation where an asymmetric stationary solution with $|\bar{\beta}_{\rm s}| \neq |\bar{\beta}_{\rm i}|$ borns (as we have checked numerically). This bifurcation is similar to the one introduced in [34], where we studied the effects of a signal injection in the two-transverse-mode DOPO, and can be understood as a switching on of the dark mode. However, note that in this case the fluctuations of the bright and dark modes are not decoupled below threshold, see the linear stability matrix (24), what physically means that the quantum properties of the dark mode at the bifurcation will be different from those of the dark mode in [34], and hence no perfect squeezing is likely to be found, as we show later.

As for the second polynomial, its roots are given by

$$\lambda_{\pm}^{\rm II} = \sigma - 1 - 2I \pm \sqrt{I^2 - \Delta^2}. \tag{27}$$

Note that $\lambda_{\pm}^{\rm II} = 0$ for $I = I_{\pm}$, that is, the turning points of the S-shaped curve correspond to bifurcation points, as must be. It is then simple to check (for example numerically) that the whole middle branch connecting this instability points is unstable, a characteristic trade of intensity-bistable systems (see figures 2(c), (d)).

But $\lambda_{\pm}^{\rm II}$ has yet one more instability when

$$I = \frac{\sigma - 1}{2} \equiv I_{\rm HB}, \tag{28}$$

provided $1 < \sigma < 1 + 2\Delta$. At this instability the eigenvalues become purely imaginary, in particular, $\lambda_{\pm}^{\rm II} = \pm{\rm i}\omega_{\rm HB}$ with $\omega_{\rm HB} = \sqrt{\Delta^2 - (\sigma-1)^2/4}$, and hence it corresponds to a Hopf bifurcation. It is simple to check that $I_{\rm HB}$ is always below $I_{\rm PB}$ and I_-; in particular, it is born at $I = 0$ for $\sigma = 1$, and climbs the $\mathcal{P}$–I curve as σ increases until it dies at $I = I_-$ for $\sigma = 1 + 2\Delta$ (see figures 2(b)–(d)). The portion of the curve with $I < I_{\rm HB}$ is unstable, and no stationary solutions can be found there, as the stable states correspond in this case to periodic orbits (as we have checked numerically, see figures 2(b)–(d)). This is also quite intuitive because, when no injection is present ($\mathcal{P} = 0$), we know that the stable states of the OPO above threshold are the ones with the signal and idler beams oscillating at the nondegenerate frequencies $\omega_0 \pm \gamma_{\rm s}$ which in the picture we are working on means $\beta_{\rm s}(\tau) \propto \exp(-{\rm i}\Delta\tau)$ and $\beta_{\rm i}(\tau) \propto \exp({\rm i}\Delta\tau)$.

This analysis proves that there exist regions in the parameter space where the frequencies of the signal and idler beams are locked to the degenerate one, and hence active locking can be a good alternative to the self-locking technique already proposed for type II OPOs [29–31].

4. Quantum properties

As explained in the introduction, in the absence of subharmonic injection ($\mathcal{P} = 0$), it is well known that there is perfect entanglement between the signal and idler modes for $\sigma = 1$ within the linearized description; above this threshold, the entanglement level is degraded (although perfect amplitude correlations persist), and the signal and idler fields start oscillating at different frequencies. Our main intention with the injection was to lock these

frequencies to the degenerate one, ω_0, which should contribute to make the observation and use of their entanglement simpler, since we will show the entanglement to be equivalent to squeezing in a couple of modes with well defined frequency and orthogonal polarization. We expect the presence of the injection to degrade the entanglement level, since it breaks the phase invariance of the OPO, and in this section we are going to evaluate how fragile the entanglement is to this injection, proving that large entanglement can still be attained.

In order to analyze the quantum properties of the system, let us first move again to the basis defined by the bright and dark modes, $\varepsilon_{\rm b} = \varepsilon_{\varphi}$ and $\varepsilon_{\rm d} = \varepsilon_{\varphi-\pi/2}$. The stochastic amplitudes associated to these modes satisfy the Langevin equations

$$\dot{\beta}_{\rm b} = \sqrt{2\mathcal{P}}\cos\varphi - \beta_{\rm b} - \Delta\beta_{\rm d} + \tilde{\beta}_{\rm p}\beta_{\rm b}^{+} + g\sqrt{\tilde{\beta}_{\rm p}}\,\eta_{\rm b}(\tau), \tag{29a}$$

$$\dot{\beta}_{\rm b}^{+} = \sqrt{2\mathcal{P}}\cos\varphi - \beta_{\rm b}^{+} - \Delta\beta_{\rm d}^{+} + \tilde{\beta}_{\rm p}^{+}\beta_{\rm b} + g\sqrt{\tilde{\beta}_{\rm p}^{+}}\,\eta_{\rm b}^{+}(\tau), \tag{29b}$$

$$\dot{\beta}_{\rm d} = \sqrt{2\mathcal{P}}\sin\varphi - \beta_{\rm d} + \Delta\beta_{\rm b} + \tilde{\beta}_{\rm p}\beta_{\rm d}^{+} + g\sqrt{\tilde{\beta}_{\rm p}}\,\eta_{\rm d}(\tau), \tag{29c}$$

$$\dot{\beta}_{\rm d}^{+} = \sqrt{2\mathcal{P}}\sin\varphi - \beta_{\rm d}^{+} + \Delta\beta_{\rm b}^{+} + \tilde{\beta}_{\rm p}^{+}\beta_{\rm d} + g\sqrt{\tilde{\beta}_{\rm p}^{+}}\,\eta_{\rm d}^{+}(\tau), \tag{29d}$$

where $\tilde{\beta}_{\rm p} = \sigma - (\beta_{\rm b}^2 + \beta_{\rm d}^2)/2$, $\tilde{\beta}_{\rm p}^{+} = \sigma - (\beta_{\rm b}^{+2} + \beta_{\rm d}^{+2})/2$, and

$$\eta_{\rm b}(\tau) = \frac{1}{\sqrt{2}}[{\rm e}^{-{\rm i}\varphi}\eta(\tau) + {\rm e}^{{\rm i}\varphi}\eta^{*}(\tau)], \tag{30a}$$

$$\eta_{\rm d}(\tau) = \frac{\rm i}{\sqrt{2}}[{\rm e}^{-{\rm i}\varphi}\eta(\tau) - {\rm e}^{{\rm i}\varphi}\eta^{*}(\tau)], \tag{30b}$$

$$\eta_{\rm b}^{+}(\tau) = \frac{1}{\sqrt{2}}[{\rm e}^{{\rm i}\varphi}\eta^{+}(\tau) + {\rm e}^{-{\rm i}\varphi}\eta^{+*}(\tau)], \tag{30c}$$

$$\eta_{\rm d}^{+}(\tau) = -\frac{\rm i}{\sqrt{2}}[{\rm e}^{{\rm i}\varphi}\eta^{+}(\tau) - {\rm e}^{-{\rm i}\varphi}\eta^{+*}(\tau)], \tag{30d}$$

behave as real independent white Gaussian noises, that is, defining $\boldsymbol{\eta}(\tau) = {\rm col}[\eta_{\rm b}(\tau),\ \eta_{\rm b}^{+}(\tau),\ \eta_{\rm d}(\tau),\ \eta_{\rm d}^{+}(\tau)]$, we have

$$\langle \eta_j(\tau)\eta_l(\tau')\rangle = \delta_{jl}\delta(\tau - \tau'). \tag{31}$$

Next, we expand the amplitudes as $\beta_{\rm b} = \sqrt{2I} + b_{\rm b}$, $\beta_{\rm b}^{+} = \sqrt{2I} + b_{\rm b}^{+}$, $\beta_{\rm d} = b_{\rm d}$, and $\beta_{\rm d}^{+} = b_{\rm d}^{+}$, and linearize the equations to first order in the fluctuations and noises, obtaining the linear system

$$\dot{\mathbf{b}} = \mathcal{L}\mathbf{b} + g\sqrt{\sigma - I}\,\boldsymbol{\eta}(\tau), \tag{32}$$

where $\mathbf{b} = {\rm col}(b_{\rm b},\ b_{\rm b}^{+},\ b_{\rm d},\ b_{\rm d}^{+})$. In appendix A.1 we solve this linear problem by finding the eigensystem associated to the linear stability matrix $\mathcal{L}$, from which we can evaluate any noise spectrum we want.

4.1. Entanglement and squeezing at the locking point

Let us now analyze the entanglement at the locking point. For $1 < \sigma < 1 + 2\Delta$ the Hopf bifurcation is the natural locking point, since it is the point with which the periodic orbits connect with the stationary solution as the injection parameter $\mathcal{P}$ is increased (see figures 2(b), (c)). On the other hand, for $\sigma > 1 + 2\Delta$ the Hopf bifurcation ceases to exist, and the periodic orbits connect directly with the upper turning point (see figure 2(d)). In both cases, the method used to solve the linear problem in appendix A.1 shows that optimal noise reduction appears in the $\varepsilon_{\varphi\pm\pi/4}$ polarization modes, which is consistent with the fact that the solutions around the locking point are symmetric in the sense of equation (19). The corresponding noise spectra are found to be

$$V^{\rm out}(\hat{Y}_{\varphi\pm\pi/4};\,\Omega) = 1 - f_{\pm}(1+\sigma), \tag{33a}$$

$$V^{\rm out}(\hat{X}_{\varphi\pm\pi/4};\,\Omega) = 1 + f_{\pm}(2I + 1 - \sigma), \tag{33b}$$

where

$$f_{\pm}(z) = \frac{4(\sigma - I)[(I \pm \Delta)^2 + z^2 + \Omega^2]}{(\Delta^2 - I^2 + z^2)^2 + 2(I^2 - \Delta^2 + z^2)\Omega^2 + \Omega^4}. \tag{34}$$

As we show below, these equations predict squeezing in the $\hat{Y}_{\varphi\pm\pi/4}$ quadratures.

Before analyzing in detail the squeezing levels that can be derived from these expressions at the locking points, it is interesting to understand their connection to entanglement. It is simple to check that the following relations hold:

$$x_{\varphi+\pi/4} = (x_{\rm s}^{\varphi+\pi/4} + x_{\rm i}^{-\varphi-\pi/4})/\sqrt{2}, \tag{35a}$$

$$y_{\varphi-\pi/4} = (x_{\rm s}^{\varphi+\pi/4} - x_{\rm i}^{-\varphi-\pi/4})/\sqrt{2}, \tag{35b}$$

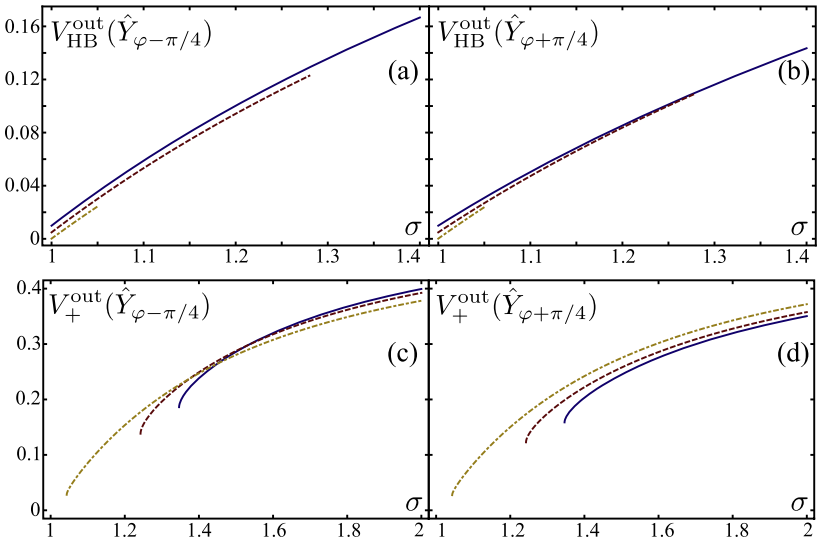

Figure 3. Noise spectra at zero frequency for the $\hat{Y}$ quadrature of the $\varepsilon_{\varphi\pm\pi/4}$ modes at the Hopf bifurcation (up) and the upper turning point (down), as a function of the pump parameter σ. Three values of Δ are considered: 0.2 (solid blue), 0.14 (dashed red), and 0.025 (dotted-dashed yellow), the last one corresponding to the value obtained in [28].

$$y_{\varphi+\pi/4} = (y_{\rm s}^{\varphi+\pi/4} + y_{\rm i}^{-\varphi-\pi/4})/\sqrt{2}, \tag{35c}$$

$$x_{\varphi-\pi/4} = (y_{\rm i}^{-\varphi-\pi/4} - y_{\rm s}^{\varphi+\pi/4})/\sqrt{2}, \tag{35d}$$

which show that squeezing in the quadratures of the $\varepsilon_{\varphi\pm\pi/4}$ modes imply quantum correlations between the quadratures of signal and idler. Indeed, whenever the condition

$$V^{\rm out}\left(\frac{\hat{X}_{\rm s}^{\varphi_{\rm s}} - \hat{X}_{\rm i}^{\varphi_{\rm i}}}{\sqrt{2}};\,\Omega\right) + V^{\rm out}\left(\frac{\hat{Y}_{\rm s}^{\varphi_{\rm s}} + \hat{Y}_{\rm i}^{\varphi_{\rm i}}}{\sqrt{2}};\,\Omega\right) < 2, \tag{36}$$

is satisfied for some phases $\varphi_{\rm s}$ and $\varphi_{\rm i}$, it implies that the state of signal and idler is not separable [18, 39, 40], which in our case is achieved because the quadratures $\hat{Y}_{\varphi\pm\pi/4}$ are squeeezed, as we show next.

Let us first point out that equation (33*a*) predicts maximum squeezing at zero noise frequency ($\Omega = 0$), both for the Hopf bifurcation and the upper turning point. In the case of the Hopf bifurcation, the noise spectra at zero frequency take the particular form

$$V_{\rm HB}^{\rm out}(\hat{Y}_{\varphi\pm\pi/4}) = 1 - \frac{8(1+\sigma)[(3+\sigma)^2 + 2(\sigma\pm\Delta)^2 + 2(1\mp\Delta)^2]}{[(3+\sigma)(1+3\sigma) + 4\Delta^2]^2}, \tag{37a}$$

$$V_{\rm HB}^{\rm out}(\hat{X}_{\varphi\pm\pi/4}) = \frac{(3+\sigma)^2 + 4\Delta^2 \pm 4\Delta(\sigma-1)}{(\sigma - 1 \pm 2\Delta)^2}. \tag{37b}$$

On the other hand, in the case of the upper turning point the corresponding expressions read

$$V_{+}^{\rm out}(\hat{Y}_{\varphi\pm\pi/4}) = 1 - \frac{4(\sigma - I_+)[(I_+ \pm \Delta)^2 + (1+\sigma)^2]}{[\Delta^2 - I_+^2 + (1+\sigma)^2]^2}, \tag{38a}$$

$$V_{+}^{\rm out}(\hat{X}_{\varphi\pm\pi/4}) = +\infty. \tag{38b}$$

Note that all these expressions predict squeezing in the $\hat{Y}$ quadratures of the $\varepsilon_{\varphi\pm\pi/4}$ modes; now, taking into account that the mean field value of these modes is $\bar{\beta}_{\varphi\pm\pi/4} = \sqrt{I} \in \mathbb{R}$, this corresponds to phase-squeezing. In practical terms, this means that, in order to capture the optimal noise reduction, homodyne detection must be performed with a local oscillator whose phase differs by $\pi/2$ from the one of the pump field.

In figure 3 we show the noise spectrum at zero frequency of these squeezed quadratures $\hat{Y}_{\varphi\pm\pi/4}$ evaluated in the aforementioned critical points as a function of the pump injection σ, and for three different values of the detuning Δ. Note that large levels of squeezing are obtained in the Hopf bifurcation even when working up to 44% above threshold ($\sigma^2 = 1.44$).

Let us finally point out an interesting property of the noise spectra (33) evaluated at the Hopf bifurcation. It is simple to show that, as usual in these type of bifurcations, maximum antisqueezing is found at the Hopf frequency, that is, $V^{\rm out}(\hat{X}_{\varphi\pm\pi/4};\,\omega_{\rm HB}) = \infty$. However, in contrast to many other nonlinear quantum optical systems, maximum squeezing is not found at the Hopf frequency but at zero noise frequency.

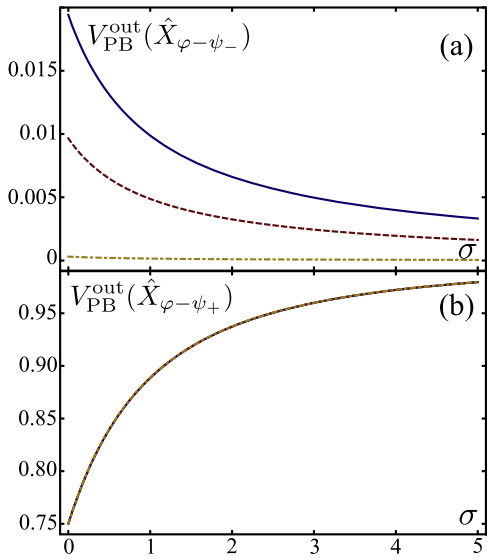

Figure 4. Noise spectra at zero frequency for the $\hat{X}$ quadrature of the $\varepsilon_{\varphi-\psi_\pm}$ polarization modes at the pitchfork bifurcation, for the same values of Δ as in the previous figure. Note that the mode $\varepsilon_{\varphi-\psi_-}$ has large amplitude squeezing for any detuning, while the mode $\varepsilon_{\varphi-\psi_+}$ does not have too much squeezing and is basically independent of the detuning.

4.2. Squeezing at the pitchfork bifurcation

Another interesting point is the pitchfork bifurcation in which the symmetric solution disappears in favor of another stationary, asymmetric solution, see figure 2. As we already pointed out, in contrast to the injected two-transverse-mode DOPO [34], we expect perfect squeezing not to appear at this bifurcation, because the fluctuations of the dark mode are not decoupled from those of the bright mode below the corresponding threshold. Nevertheless, we prove in this section that large squeezing levels are still attainable.

The first thing to note in this case is that the method we use to solve the linearized equations (32) shows that, at the pitchfork bifurcation, optimal squeezing noise reduction appears in the polarization basis $\varepsilon_{\varphi-\psi_\pm}$, where $\psi_\pm = \pi/4 \pm \arg\{I - \Delta + \sqrt{I^2 - \Delta^2} + \mathrm{i}(I - \Delta + \sqrt{I^2 - \Delta^2})\}$. While it seems difficult to understand the physical origin of these phases, we are convinced that it is rooted in the fact that the solution above this bifurcation is not symmetric anymore in the sense of equations (19). As shown in appendix A.1, in this basis we get the zero-noise-frequency noise spectra (again, squeezing is optimal at $\Omega = 0$)

$$V_{\rm PB}^{\rm out}(\hat{X}_{\varphi-\psi_-}) = 1 - \frac{1}{I_{\rm PB} - \sigma}, \tag{39a}$$

$$V_{\rm PB}^{\rm out}(\hat{Y}_{\varphi-\psi_-}) = +\infty, \tag{39b}$$

$$V_{\rm PB}^{\rm out}(\hat{X}_{\varphi-\psi_+}) = 1 - \frac{I_{\rm PB} - \sigma}{(1 + I_{\rm PB})^2}, \tag{39c}$$

$$V_{\rm PB}^{\rm out}(\hat{Y}_{\varphi-\psi_+}) = 1 + \frac{I_{\rm PB} - \sigma}{(\sigma + 1)^2}. \tag{39d}$$

In this case the $\hat{Y}$ quadrature of the $\varepsilon_{\varphi-\psi_-}$ mode is perfectly antisqueezed; its complementary, the $\hat{X}$ quadrature of the same mode, is not perfectly squeezed, but it shows very high noise reduction, as shown in figure 4(a). On the other hand, the $\varepsilon_{\varphi-\psi_+}$ polarization mode shows also noise reduction in its $\hat{X}$ quadrature, although the squeezing levels are quite modest in this case, see figure 4(b).

We can understand much better the dependence of these spectra on the parameters by performing expansions to the leading order in the detuning (note in particular that the one corresponding to the $\varepsilon_{\varphi-\psi_+}$ is independent of the detuning):

$$V_{\rm PB}^{\rm out}(\hat{X}_{\varphi-\psi_-}) \approx \frac{\Delta^2}{2(\sigma + 1)}, \tag{40a}$$

$$V_{\rm PB}^{\rm out}(\hat{X}_{\varphi-\psi_+}) \approx 1 - \frac{1}{(\sigma + 2)^2}. \tag{40b}$$

Note finally that, in this polarization basis, the steady-state solution reads $\bar{\beta}_{\varphi-\psi_\pm} = \sqrt{2I_{\rm PB}}\cos\psi_\pm \in \mathbb{R}$, and hence, in this case the squeezed quadrature is aligned with the phase of the classical solution (amplitude

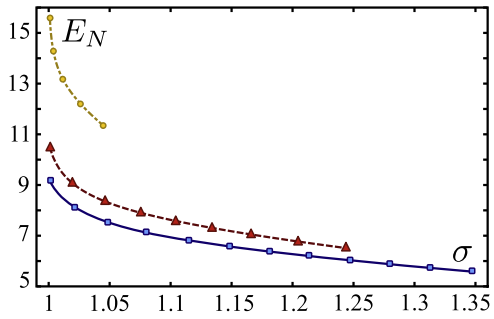

Figure 5. Logarithmic negativity (E_N) as a function of the pump parameter σ at the Hopf bifurcation, which corresponds to the minimum value of the injection $\mathcal{P}$ for which the oscillation frequencies of signal and idler get locked. The solid curves correspond to the analytical solution that we found for the symmetric case within the linearized theory, while the markers are found numerically for the asymmetric example detailed in the text. Three values of Δ have been chosen, coinciding with the ones in the previous figures: 0.2 (solid blue, squares), 0.14 (dashed red, triangles) and 0.025 (dashed-dotted yellow, circles).

squeezing), contrary to what happens at the locking points. In practical terms, now this means that the local oscillator must be in phase with the pump to observe optimal noise reduction.

5. Beyond the symmetric case

In order to get analytical insight, in the previous sections we have focused in the case in which signal and idler are detuned symmetrically with respect to the subharmonic injection at frequency ω_0. In real experiments, however, it is extremely challenging to meet such a symmetric configuration, since it requires unfeasible fine tuning. Hence, in order for our locking method to be of use, it is important to study whether our predictions persist when working out of such a symmetric situation, and this is what we prove in this section. The main difficulty when working out of the symmetric configuration is that we do not have an analytic solution and stability analysis to rely on, and hence, we need to resort to numerical tools. Using these, we will show though that the Hopf instability is still present in the asymmetric case, as well as large levels of entanglement between signal and idler.

Our starting point is again the normalized equations in which the pump has been adiabatically eliminated, equation (10), but allowing for general signal and idler detuning, which amounts to replace Δ by Δ_s in equations (10*a*) and (10*b*), and by $-\Delta_i$ in equations (10*c*) and (10*d*). The first step consists in finding the classical configuration of the system, what we do numerically in this case. In particular, we first check that even in this asymmetric configuration, the classical version of this equations still possess a Hopf bifurcation above threshold ($\sigma > 1$). To this aim, at a given value of the pump parameter σ, we start from an injection $\mathcal{P}$ large enough so that the system reaches a stationary solution $\bar{\beta}_{s,i}$, and then decrease the injection gradually until the real part of one of the eigenvalues of the linear stability matrix gets as close to zero as we desire, checking that the imaginary part of the eigenvalue is non-zero. This proves that the Hopf instability is still present in this asymmetric case, and, moreover, we have checked that if we keep decreasing the injection, periodic orbits are found as the asymptotic solution of the system. Hence, again we see that above threshold it is required a minimum value of the injection to lock the signal and idler frequencies.

Once we have identified the Hopf bifurcation, which we remind it is the natural locking point of the system, we compute its quantum properties by linearizing the Langevin equations, similarly to the symmetric case. However, in this case we find the eigensystem of the linear stability matrix numerically for each parameter set. As explained in detail in appendix A.2, from this eigensystem we can compute the output field's spectral covariance matrix in the signal/idler basis, and compute from it the logarithmic negativity quantifying the entanglement between these two modes following standard Gaussian techniques [17, 18]. We provide all the details in appendix A.2 as well, and here we just want to compare these levels to the ones obtained in the symmetric case.

We have made an exhaustive analysis of the logarithmic negativity as a function of the signal and idler detunings, concluding that the entanglement properties of the system depend only on the distance between the signal and idler resonances, and not on how they are disposed with respect to the frequency of the subharmonic injection, which is a most important conclusion for experiments. This is shown in figure 5 for some selected examples. In particular, we choose some distance between the signal and idler resonances, say $2\Delta > 0$, which in the symmetric case means $\Delta_s = -\Delta_i = \Delta$, while we choose $\Delta_s = \Delta + \Delta/2$ and $\Delta_i = -\Delta + \Delta/2$ as a highly asymmetric example. In figure 5 we then plot the logarithmic negativity as a function of σ for different values of Δ. Remarkably, we can see that, not only the entanglement levels are also high in the asymmetric case, but they coincide within the numerical accuracy with the ones of the symmetric case.

6. Conclusion

In this work we have put forward a method to obtain exact frequency degeneracy in type II OPOs, which is based on the injection of a laser field at half the frequency of the pump laser. We have studied the impact that such subharmonic injection has on the entanglement generated on the down-converted fields, proving that large quantum correlations are still present at the locking region. Hence, this technique offers an easily tunable alternative to more invasive techniques which require the introduction of additional optical elements in the cavity. Apart from large levels of entanglement at the locking bifurcation, we have also identified an additional (static) instability where a high level of amplitude squeezing is obtained.

Let us remark that we have also analyzed the case in which the subharmonic injection is not in phase with the pump beam (amplification regime), but is phase-shifted by $\pi/2$ (attenuation regime), finding similar results that will be shown elsewhere.

Finally, we find it relevant to point out the relation of our work to the field of synchronization, which has received a lot of attention lately in the context of modern quantum-optical platforms [41–63]. In the regime of interest to our work, synchronization between the signal and idler modes occurs only at the classical level [64], but it has a strong influence on how quantum fluctuations are distributed around such synchronized classical states. An interesting future venue may consist on studying the limits that quantum mechanics impose to signal-idler synchronization, or considering deeper quantum regimes of the system where signatures of quantum synchronization could arise.

Acknowledgments

We have benefited from discussions with: Claude Fabre, Raúl García-Patrón, Eugenio Roldán, Talitha Weiss, Andrea Mari, and Géza Giedke. This work has been supported by the Spanish Government and the European Union FEDER through Projects FIS2011-26960 and FIS2014-60715-P. CN-B acknowledges support from the ERC OPTOMECH and the Alexander von Humboldt foundation through its fellowship for postdoctoral researchers.

Appendix. Manipulating the linearized Langevin equations

Our analysis of the quantum properties of the down-converted field was based on the linearized Langevin equations. In this appendix we will show explicitly how we have dealt with these equations in order to obtain the quantities of interest, both in the symmetric and asymmetric cases. Conceptually, the approach we use is the same in the symmetric and asymmetric cases: we solve the linear system by making use of the eigensystem of the stability matrix. However, in the symmetric case we will be able to find the eigensystem analytically, while in the asymmetric case only numerically. Let us then start by commenting on some general aspects, and then particularize to our problems at hand.

In general, the linearized Langevin equations can be written in the form

$$\dot{\mathbf{b}} = \mathcal{L}\mathbf{b} + g\sqrt{|\bar{\beta}_{\rm p}|}\,\boldsymbol{\eta}(\tau). \tag{A.1}$$

In this expression $\bar{\beta}_{\rm p} = \sigma - \bar{\beta}_{\rm s}\bar{\beta}_{\rm i}$, $\mathbf{b}$ is a vector containing the quantum fluctuations of the stochastic amplitudes in the polarization basis that we choose to write the equations on, $\mathcal{L}$ is the corresponding linear stability matrix, and we assume that the components of the noise vector obey the two-time correlators $\langle \eta_m(\tau)\eta_n(\tau')\rangle = \mathcal{S}_{mn}\delta(\tau - \tau')$, with $\mathcal{S}$ some matrix.

Given this equation, we proceed by finding the left eigenvectors $\{\mathbf{u}_j\}_{j=1,2,3,4}$ defined by $\mathbf{u}_j^\dagger\mathcal{L} = \lambda_j\mathbf{u}_j^\dagger$ or, equivalently, $\mathcal{L}^\dagger\mathbf{u}_j = \lambda_j^*\mathbf{u}_j$ (note that they are defined as column vectors). The corresponding eigenvalues are denoted by λ_j. Acting on equation (A.1) with $\mathbf{u}_j^\dagger$ on the left, and defining the projections $c_j(\tau) = \mathbf{u}_j^\dagger\mathbf{b}(\tau)$, we obtain

$$\dot{c}_j = \lambda_j c_j + g\sqrt{|\bar{\beta}_{\rm p}|}\,\mathbf{u}_j^\dagger\boldsymbol{\eta}(\tau), \tag{A.2}$$

which has the asymptotic ($\tau \gg -\mathrm{Re}\{\lambda_j\}^{-1}\ \forall j$) solution

$$c_j(\tau) = g\sqrt{|\bar{\beta}_{\rm p}|}\int_0^\tau \mathrm{d}\tau e^{\lambda_j(\tau-\tau')}\mathbf{u}_j^\dagger\boldsymbol{\eta}(\tau'), \tag{A.3}$$

leading to the asymptotic correlation functions

$$\langle c_j(\tau)c_l(\tau')\rangle = -\frac{g^2|\bar{\beta}_{\rm p}|\mathbf{u}_j^\dagger \mathcal{S}\mathbf{u}_l^*}{\lambda_j+\lambda_l} \times \begin{cases} e^{\lambda_l(\tau'-\tau)} & \tau'>\tau \\ e^{\lambda_j(\tau-\tau')} & \tau'<\tau \end{cases} \tag{A.4}$$

and ultimately to the asymptotic spectra

$$\mathcal{C}_{jl}(\Omega) = \lim_{\tau\to\infty}\int_{-\infty}^{+\infty} d\tau' e^{-i\Omega\tau'}\langle c_j(\tau)c_l(\tau+\tau')\rangle = \frac{g^2|\bar{\beta}_{\rm p}|\mathbf{u}_l^\dagger \mathcal{S}\mathbf{u}_j^*}{(\lambda_j+i\Omega)(\lambda_l-i\Omega)}, \tag{A.5}$$

which define a matrix $\mathcal{C}$. The noise spectrum (14) of any quadrature, or even more complicated objects such as the spectral covariance matrix in any polarization basis, can be evaluated by making a proper combination of these spectra, as we will see shortly.

A.1. Symmetric configuration

In the case of the symmetric configuration, the linearized Langevin equations take the form (32) in the bright/dark basis, leading to $|\bar{\beta}_{\rm p}| = \sigma - I$, $\mathcal{S} = \mathbb{1}$, where $\mathbb{1}$ is the identity matrix, and a linear stability matrix $\mathcal{L}$ given by equation (24). In order to apply the general expressions above in this symmetric configuration, it is convenient to analyze separately the cases $I<\Delta$ and $I>\Delta$, since $\mathcal{L}$ becomes singular at $I=\Delta$.

A.1.1. Eigensystem and noise spectra for $I<\Delta$. In the $I<\Delta$ case, the eigenvalues read

$$\lambda_1 = -1-\sigma-i\sqrt{\Delta^2-I^2}, \tag{A.6a}$$

$$\lambda_2 = -1-\sigma+i\sqrt{\Delta^2-I^2}, \tag{A.6b}$$

$$\lambda_3 = -1+\sigma-2I-i\sqrt{\Delta^2-I^2}, \tag{A.6c}$$

$$\lambda_4 = -1+\sigma-2I+i\sqrt{\Delta^2-I^2}, \tag{A.6d}$$

with corresponding left eigenvectors

$$\mathbf{u}_1 = \mathrm{col}(e^{-i\phi/2}, -e^{-i\phi/2}, e^{i\phi/2}, -e^{i\phi/2}), \tag{A.7a}$$

$$\mathbf{u}_2 = \mathrm{col}(e^{i\phi/2}, -e^{i\phi/2}, e^{-i\phi/2}, -e^{-i\phi/2}), \tag{A.7b}$$

$$\mathbf{u}_3 = \mathrm{col}(e^{-i\phi/2}, e^{-i\phi/2}, e^{i\phi/2}, e^{i\phi/2}), \tag{A.7c}$$

$$\mathbf{u}_4 = \mathrm{col}(e^{i\phi/2}, e^{i\phi/2}, e^{-i\phi/2}, e^{-i\phi/2}), \tag{A.7d}$$

where $\phi = \arg\{I+i\sqrt{\Delta^2-I^2}\}$.

Since the eigenvalues are complex, it is clear that the projections c_j cannot be directly proportional to observable quantities. However, one can easily show that simple combinations of them are indeed proportional to the quadratures of the $\varepsilon_{\varphi\pm\pi/4}$ polarization modes:

$$c_1+c_2 = 2i\sqrt{1+I/\Delta}\,\delta y_{\varphi-\pi/4}, \tag{A.8a}$$

$$c_1-c_2 = -2\sqrt{1-I/\Delta}\,\delta y_{\varphi+\pi/4}, \tag{A.8b}$$

$$c_3+c_4 = 2\sqrt{1+I/\Delta}\,\delta x_{\varphi-\pi/4}, \tag{A.8c}$$

$$c_3-c_4 = 2i\sqrt{1-I/\Delta}\,\delta x_{\varphi+\pi/4}. \tag{A.8d}$$

Hence, we get the noise spectra

$$V^{\rm out}(\hat{Y}_{\varphi-\pi/4};\Omega) = 1-\frac{\mathcal{C}_{11}(\Omega)+\mathcal{C}_{22}(\Omega)+\mathcal{C}_{21}(\Omega)+\mathcal{C}_{12}(\Omega)}{2g^2(1+I/\Delta)}, \tag{A.9a}$$

$$V^{\rm out}(\hat{Y}_{\varphi+\pi/4};\Omega) = 1+\frac{\mathcal{C}_{11}(\Omega)+\mathcal{C}_{22}(\Omega)-\mathcal{C}_{21}(\Omega)-\mathcal{C}_{12}(\Omega)}{2g^2(1-I/\Delta)}, \tag{A.9b}$$

$$V^{\rm out}(\hat{X}_{\varphi-\pi/4};\Omega) = 1+\frac{\mathcal{C}_{33}(\Omega)+\mathcal{C}_{44}(\Omega)+\mathcal{C}_{34}(\Omega)+\mathcal{C}_{43}(\Omega)}{2g^2(1+I/\Delta)}, \tag{A.9c}$$

$$V^{\rm out}(\hat{X}_{\varphi+\pi/4};\Omega) = 1-\frac{\mathcal{C}_{33}(\Omega)+\mathcal{C}_{44}(\Omega)-\mathcal{C}_{34}(\Omega)-\mathcal{C}_{43}(\Omega)}{2g^2(1-I/\Delta)}. \tag{A.9d}$$

These spectra have actually fairly simple analytical expressions in terms of the system parameters, expressions that we gave explicitly in equation (33) in the main text.

A.1.2. Eigensystem and noise spectra for $I>\Delta$. In the $I>\Delta$ case, defining the functions $F_\pm = I\pm\sqrt{I^2-\Delta^2}>0$, the left eigensystem of $\mathcal{L}$ is easily found to be

$$\mathbf{u}_1 = \mathrm{col}(F_+, -F_+, \Delta, -\Delta), \tag{A.10a}$$

$$\mathbf{u}_2 = \mathrm{col}(F_-, -F_-, \Delta, -\Delta), \tag{A.10b}$$

$$\mathbf{u}_3 = \mathrm{col}(F_+, F_+, \Delta, \Delta), \tag{A.10c}$$

$$\mathbf{u}_4 = \mathrm{col}(F_-, F_-, \Delta, \Delta), \tag{A.10d}$$

with corresponding eigenvalues

$$\lambda_1 = -1 - \sigma - \sqrt{I^2 - \Delta^2}, \tag{A.11a}$$

$$\lambda_2 = -1 - \sigma + \sqrt{I^2 - \Delta^2}, \tag{A.11b}$$

$$\lambda_3 = -1 + \sigma - 2I - \sqrt{I^2 - \Delta^2}, \tag{A.11c}$$

$$\lambda_4 = -1 + \sigma - 2I + \sqrt{I^2 - \Delta^2}. \tag{A.11d}$$

Let us define the amplitude and phase of $F_\pm + \mathrm{i}\Delta$ as $M_\pm$ and $\psi_\pm$ respectively, which can be written as

$$M_\pm = 2I(I \pm \sqrt{I^2 - \Delta^2}), \tag{A.12a}$$

$$\psi_\pm = \frac{\pi}{4} \mp \psi, \tag{A.12b}$$

with $\psi = \arg\{I - \Delta + \sqrt{I^2 - \Delta^2} + \mathrm{i}(I - \Delta + \sqrt{I^2 - \Delta^2})\}$. In this case the eigenvalues are real, and it is therefore possible to find a relation between the projections and the quadratures of modes with polarization $\varepsilon_{\varphi-\psi_\pm}$:

$$c_1 = \sqrt{M_+}\,\mathrm{i}\delta y_{\varphi-\psi_+}, \tag{A.13a}$$

$$c_2 = \sqrt{M_-}\,\mathrm{i}\delta y_{\varphi-\psi_-}, \tag{A.13b}$$

$$c_3 = \sqrt{M_+}\,\delta x_{\varphi-\psi_+}, \tag{A.13c}$$

$$c_4 = \sqrt{M_-}\,\delta x_{\varphi-\psi_-}, \tag{A.13d}$$

leading to the noise spectra

$$V^{\mathrm{out}}(\hat{Y}_{\varphi-\psi_+};\,\Omega) = 1 - \frac{2}{g^2 M_+}\mathcal{C}_{11}(\Omega) = 1 - \frac{4(\sigma - I)}{(1 + \sigma + \sqrt{I^2 - \Delta^2})^2 + \Omega^2}, \tag{A.14a}$$

$$V^{\mathrm{out}}(\hat{Y}_{\varphi-\psi_-};\,\Omega) = 1 - \frac{2}{g^2 M_-}\mathcal{C}_{22}(\Omega) = 1 - \frac{4(\sigma - I)}{(1 + \sigma - \sqrt{I^2 - \Delta^2})^2 + \Omega^2}, \tag{A.14b}$$

$$V^{\mathrm{out}}(\hat{X}_{\varphi-\psi_+};\,\Omega) = 1 + \frac{2}{g^2 M_+}\mathcal{C}_{33}(\Omega) = 1 + \frac{4(\sigma - I)}{(1 - \sigma + 2I + \sqrt{I^2 - \Delta^2})^2 + \Omega^2}, \tag{A.14c}$$

$$V^{\mathrm{out}}(\hat{X}_{\varphi-\psi_-};\,\Omega) = 1 + \frac{2}{g^2 M_-}\mathcal{C}_{44}(\Omega) = 1 + \frac{4(\sigma - I)}{(1 - \sigma + 2I - \sqrt{I^2 - \Delta^2})^2 + \Omega^2}. \tag{A.14d}$$

This expressions, particularized to $\Omega = 0$ and the pitchfork bifurcation $I = I_{\mathrm{PB}}$ are the ones we gave in equation (39).

In order to compare with the $I < \Delta$ case, it is also convenient to analyze the noise spectra in the $\varepsilon_{\varphi\pm\pi/4}$ polarization basis. For this, we now relate these mode's quadratures modes with the projections c_j. In particular, it is easy to find

$$\frac{c_1}{\sqrt{M_+}} + \frac{c_2}{\sqrt{M_-}} = \sqrt{2\left(1 + \frac{\Delta}{I}\right)}\,\mathrm{i}\delta y_{\varphi-\pi/4}, \tag{A.15a}$$

$$\frac{c_1}{\sqrt{M_+}} - \frac{c_2}{\sqrt{M_-}} = \sqrt{2\left(1 - \frac{\Delta}{I}\right)}\,\mathrm{i}\delta y_{\varphi+\pi/4}, \tag{A.15b}$$

$$\frac{c_3}{\sqrt{M_+}} + \frac{c_4}{\sqrt{M_-}} = \sqrt{2\left(1 + \frac{\Delta}{I}\right)}\,\delta x_{\varphi-\pi/4}, \tag{A.15c}$$

$$\frac{c_3}{\sqrt{M_+}} - \frac{c_4}{\sqrt{M_-}} = \sqrt{2\left(1 - \frac{\Delta}{I}\right)}\,\delta x_{\varphi+\pi/4}. \tag{A.15d}$$

where the identities $\sqrt{2}\cos\psi = \sqrt{1 + \Delta/I}$ and $\sqrt{2}\sin\psi = \sqrt{1 - \Delta/I}$ are useful when checking this relations. Hence, the noise spectrum of the corresponding quadratures can be written as

$$V^{\mathrm{out}}(\hat{Y}_{\varphi-\pi/4};\,\Omega) = 1 - \left[\frac{\mathcal{C}_{11}(\Omega)}{M_+} + \frac{\mathcal{C}_{22}(\Omega)}{M_-} + \frac{\mathcal{C}_{21}(\Omega) + \mathcal{C}_{12}(\Omega)}{\sqrt{M_+ M_-}}\right]\left[g^2\left(1 + \frac{\Delta}{I}\right)\right]^{-1}, \tag{A.16a}$$

$$V^{\rm out}(\hat{Y}_{\varphi+\pi/4};\,\Omega) = 1 - \left[\frac{\mathcal{C}_{11}(\Omega)}{M_+} + \frac{\mathcal{C}_{22}(\Omega)}{M_-} - \frac{\mathcal{C}_{21}(\Omega)+\mathcal{C}_{12}(\Omega)}{\sqrt{M_+M_-}}\right]\left[g^2\left(1-\frac{\Delta}{I}\right)\right]^{-1}, \tag{A.16b}$$

$$V^{\rm out}(\hat{X}_{\varphi-\pi/4};\,\Omega) = 1 + \left[\frac{\mathcal{C}_{33}(\Omega)}{M_+} + \frac{\mathcal{C}_{44}(\Omega)}{M_-} + \frac{\mathcal{C}_{34}(\Omega)+\mathcal{C}_{43}(\Omega)}{\sqrt{M_+M_-}}\right]\left[g^2\left(1+\frac{\Delta}{I}\right)\right]^{-1}, \tag{A.16c}$$

$$V^{\rm out}(\hat{X}_{\varphi+\pi/4};\,\Omega) = 1 + \left[\frac{\mathcal{C}_{33}(\Omega)}{M_+} + \frac{\mathcal{C}_{44}(\Omega)}{M_-} - \frac{\mathcal{C}_{34}(\Omega)+\mathcal{C}_{43}(\Omega)}{\sqrt{M_+M_-}}\right]\left[g^2\left(1-\frac{\Delta}{I}\right)\right]^{-1}. \tag{A.16d}$$

It is again easy to check that, in terms of the system parameters, these combinations read as given in equation (33), and hence they coincide with the expressions found in the $I > \Delta$ case. This means that, even though the eigensystems are very different in the $I > \Delta$ and $I < \Delta$ cases, and furthermore the matrix $\mathcal{L}$ cannot be diagonalized in the $I = \Delta$ limit, this mathematical pathology is not present in the physical observables. This is indeed characteristic of detuned nonlinear quantum-optical cavities.

A.2. Asymmetric configuration

In the case of the asymmetric configuration, we work in the signal/idler basis, where we find the classical solution $\bar{\beta}_{\rm s,i}$ numerically as explained in the text for each choice of parameters. In this case, we then have $\mathbf{b} = \mathrm{col}(b_{\rm s},\, b_{\rm s}^+,\, b_{\rm i},\, b_{\rm i}^+)$,

$$\mathcal{L} = \begin{pmatrix} \Theta_{\rm s} & 0 & -\bar{\beta}_{\rm s}\bar{\beta}_{\rm i}^* & \sigma \\ 0 & \Theta_{\rm s}^* & \sigma & -\bar{\beta}_{\rm s}^*\bar{\beta}_{\rm i} \\ -\bar{\beta}_{\rm s}^*\bar{\beta}_{\rm i} & \sigma & \Theta_{\rm i} & 0 \\ \sigma & -\bar{\beta}_{\rm s}\bar{\beta}_{\rm i}^* & 0 & \Theta_{\rm i}^* \end{pmatrix}, \tag{A.17}$$

with $\Theta_{\rm s,i} = -1 - {\rm i}\Delta_{\rm s,i} - |\bar{\beta}_{\rm i,s}|^2$, and

$$\mathcal{S} = \begin{pmatrix} 0 & 0 & {\rm e}^{2{\rm i}\varphi_{\rm p}} & 0 \\ 0 & 0 & 0 & {\rm e}^{-2{\rm i}\varphi_{\rm p}} \\ {\rm e}^{2{\rm i}\varphi_{\rm p}} & 0 & 0 & 0 \\ 0 & {\rm e}^{-2{\rm i}\varphi_{\rm p}} & 0 & 0 \end{pmatrix}, \tag{A.18}$$

with $\varphi_{\rm p} = \arg\{\bar{\beta}_{\rm p}\}$. We find the eigensystem of $\mathcal{L}$ numerically for each choice of the system parameters.

We can characterize the quantum state of the output field by the spectral covariance matrix. Collecting the normalized stochastic quadratures of signal and idler in a vector $\mathbf{r} = (x_{\rm s},\, y_{\rm s},\, x_{\rm i},\, y_{\rm i})$, this can be evaluated as

$$\mathcal{V}(\Omega) = \mathbb{1} + \frac{2}{g^2}\int_{-\infty}^{+\infty} {\rm d}\tau \mathcal{M}(\tau){\rm e}^{-{\rm i}\Omega\tau}, \tag{A.19}$$

where the elements of the normally-ordered two-time correlation matrix $\mathcal{M}$ are given by

$$\mathcal{M}_{jl}(\tau) = \lim_{\tau'\to\infty} \frac{\langle \delta r_j(\tau')\delta r_l(\tau-\tau') + \delta r_l(\tau')\delta r_j(\tau-\tau')\rangle}{2}. \tag{A.20}$$

At the end of this section we explain how this two-mode covariance matrix allows for a characterization of the entanglement between the signal and idler modes. But before that, let us show how we can compute it from the solution that we found for the linearized problem, in particular from the spectral correlation matrix $\mathcal{C}(\Omega)$ of the projections. Note that the relation between the quadrature fluctuations $\delta\mathbf{r}$ and the quantum fluctuations $\mathbf{b}$ can be written in matrix form as $\delta\mathbf{r}(\tau) = \mathcal{R}\mathbf{b}(\tau)$ with

$$\mathcal{R} = \begin{pmatrix} 1 & 1 \\ -{\rm i} & {\rm i} \end{pmatrix} \oplus \begin{pmatrix} 1 & 1 \\ -{\rm i} & {\rm i} \end{pmatrix}, \tag{A.21}$$

while defining the vector of projections $\mathbf{c} = \mathrm{col}(c_1,\, c_2,\, c_3,\, c_4)$ and the matrix of left-eigenvectors $\mathcal{U} = \mathrm{col}(\mathbf{u}_1^\dagger,\, \mathbf{u}_2^\dagger,\, \mathbf{u}_3^\dagger,\, \mathbf{u}_4^\dagger)$, we can write $\mathbf{b}(\tau) = \mathcal{U}^{-1}\mathbf{c}(\tau)$. Hence, we see that we can write the quadrature-vector in terms of the projection-vector as $\delta\mathbf{r}(\tau) = \mathcal{R}\mathcal{U}^{-1}\mathbf{c}(\tau)$, leading to

$$\mathcal{V}(\Omega) = \mathbb{1} + \frac{1}{g^2}\mathcal{R}\mathcal{U}^{-1}[\mathcal{C}(\Omega) + \mathcal{C}^T(\Omega)]\mathcal{U}^{-1T}\mathcal{R}^T. \tag{A.22}$$

Let us remark that this expression can be efficiently evaluated numerically once we have identified the classical stationary solution at the Hopf bifurcation, $\bar{\beta}_{\rm s,i}$, from which we derive the linear stability matrix $\mathcal{L}$, its eigensystem, and from it $\mathcal{U}^{-1}$ as well as the spectral correlation matrix $\mathcal{C}(\Omega)$. In the following we take $\Omega = 0$ as this is the value of the noise frequency that leads to the largest levels of entanglement in the symmetric case.

Having the covariance matrix, we are now ready to analyze the entanglement between the signal and idler modes. In order to be numerically efficient, we choose to quantify the entanglement between these two modes

via the logarithmic negativity, which is an entanglement monotone, albeit not a proper measure [18]. Since by construction, the linearized approach generates a Gaussian state for the system, the logarithmic negativity can be easily computed from the two-mode spectral covariance matrix by following standard techniques, see for example [17, 18]. In particular, defining the partially-transposed spectral covariance matrix

$$\tilde{\mathcal{V}} = \mathcal{Z}\mathcal{V}(0)\mathcal{Z} \equiv \begin{pmatrix} A & C \\ C^T & B \end{pmatrix}, \tag{A.23}$$

where $\mathcal{Z} = \mathrm{diag}(1,\ 1,\ 1,\ -1)$, the logarithmic negativity takes the expression

$$E_{\mathrm{N}} = -\sum_{j=\pm} \begin{cases} \log \tilde{\nu}_j & \tilde{\nu}_j < 1 \\ 0 & \tilde{\nu}_j \geqslant 1 \end{cases}, \tag{A.24}$$

where $\tilde{\nu}_{\pm}$ are the symplectic eigenvalues associated to $\tilde{\mathcal{V}}$, which can be found from

$$\tilde{\nu}_{\pm}^2 = \frac{\tilde{\Delta} \pm \sqrt{\tilde{\Delta}^2 - 4 \det \tilde{\mathcal{V}}}}{2}, \tag{A.25}$$

with $\tilde{\Delta} = \det A + \det B + 2 \det C$.

References

[1] Boyd R W 2003 *Nonlinear Optics* (New York: Academic)
[2] Navarrete-Benlloch C 2011 Contributions to the quantum optics of multi-mode optical parametric oscillators *PhD Thesis* Universitat de València (arXiv:1504.05917)
[3] Meystre P and Walls D F (ed) 1991 *Nonclassical Effects in Quantum Optics* (New York: American Institute of Physics)
[4] Vahlbruch H, Mehmet M, Danzmann K and Schnabel R 2016 *Phys. Rev. Lett.* **117** 110801
[5] Mehmet M, Ast S, Eberle T, Steinlechner S, Vahlbruch H and Schnabel R 2011 *Opt. Express* **19** 25763
[6] Eberle T, Steinlechner S, Bauchrowitz J, Händchen V, Vahlbruch H, Mehmet M, Müller-Ebhardt H and Schnabel R 2010 *Phys. Rev. Lett.* **104** 251102
[7] Mehmet M, Vahlbruch H, Lastzka N, Danzmann K and Schnabel R 2010 *Phys. Rev.* A **81** 013814
[8] Vahlbruch H, Mehmet M, Chelkowski S, Hage B, Franzen A, Lastzka N, Gossler S, Danzmann K and Schnabel R 2008 *Phys. Rev. Lett.* **100** 033602
[9] Takeno Y, Yukawa M, Yonezawa H and Furusawa A 2007 *Opt. Express* **15** 4321
[10] Collett M J and Gardiner C W 1984 *Phys. Rev.* A **30** 1386
[11] Goda K, Miyakawa O, Mikhailov E E, Saraf S, Adhikari R, McKenzie K, Ward R, Vass S, Weinstein A J and Mavalvala N 2008 *Nat. Phys.* **4** 472–6
[12] Vahlbruch H, Chelkowski S, Hage B, Franzen A, Danzmann K and Schnabel R 2005 *Phys. Rev. Lett.* **95** 211102
[13] Treps N, Andersen U, Buchler B, Lam P K, Maître A, Bachor H-A and Fabre C 2002 *Phys. Rev. Lett.* **88** 203601
[14] Treps N, Grosse N, Bowen W P, Fabre C, Bachor H-A and Lam P K 2003 *Science* **301** 940
[15] Einstein A, Podolsky B and Rosen N 1935 *Phys. Rev.* **47** 777
[16] Braunstein S L and van Loock P 2005 *Rev. Mod. Phys.* **77** 513
[17] Weedbrook C, Pirandola S, García-Patrón R, Cerf N J, Ralph T C, Shapiro J H and Lloyd S 2012 *Rev. Mod. Phys.* **84** 621
[18] Navarrete-Benlloch C 2015 *An Introduction to the Formalism of Quantum Information with Continuous Variables* (Bristol: Institute of Physics Publishing)
[19] Reid M D and Drummond P D 1988 *Phys. Rev. Lett.* **60** 2731
[20] Reid M D 1989 *Phys. Rev.* A **40** 913
[21] Drummond P D and Reid M D 1990 *Phys. Rev.* A **41** 3930
[22] Lane A S, Reid M D and Walls D F 1988 *Phys. Rev.* A **38** 788
[23] Reid M D and Drummond P D 1989 *Phys. Rev.* A **40** 4493
[24] Navarrete-Benlloch C, Roldán E and de Valcárcel G J 2008 *Phys. Rev. Lett.* **100** 203601
[25] Navarrete-Benlloch C, Romanelli A, Roldán E and de Valcárcel G J 2010 *Phys. Rev.* A **81** 043829
[26] Reynaud S, Fabre C and Giacobino E 1987 *J. Opt. Soc. Am.* B **4** 1520
[27] Heidmann A, Horowicz R J, Reynaud S, Giacobino E, Fabre C and Camy G 1987 *Phys. Rev. Lett.* **59** 2555
[28] Feng S and Pfister O 2003 *J. Opt. B: Quantum Semiclass. Opt.* **5** 262
[29] Longchambon L, Laurat J, Coudreau T and Fabre C 2004 *Eur. Phys. J.* D **30** 279
[30] Longchambon L, Laurat J, Coudreau T and Fabre C 2004 *Eur. Phys. J.* D **30** 287
[31] Laurat J, Longchambon L, Fabre C and Coudreau T 2005 *Opt. Lett.* **30** 1177
[32] Garcia-Ferrer F V, Navarrete-Benlloch C, de Valcárcel G J and Roldán E 2010 *Opt. Lett.* **35** 2194
[33] Garcia-Ferrer F V, Navarrete-Benlloch C, de Valcárcel G J and Roldán E 2009 *IEEE J. Quantum Electron.* **45** 1404
[34] Navarrete-Benlloch C, Roldán E and deValcárcel G J 2011 *Phys. Rev.* A **83** 043812
[35] Navarrete-Benlloch C and de Valcárcel G J 2013 *Phys. Rev.* A **87** 065802
[36] Carmichael H J 1999 *Statistical Methods in Quantum Optics 1: Master Equations and Fokker-Planck Equations* (Berlin: Springer)
[37] Gardiner C W and Zoller P 2000 *Quantum Noise* (Berlin: Springer)
[38] Drummond P D and Gardiner C W 1980 *J. Phys. A: Math. Gen.* **13** 2353
[39] Duan L-M, Giedke G, Cirac J I and Zoller P 2000 *Phys. Rev. Lett.* **84** 2722
[40] Simon R 2000 *Phys. Rev. Lett.* **84** 2726
[41] Vinokur V M, Baturina T I, Fistul M V, Mironov A Y, Baklanov M R and Strunk C 2008 *Nature* **452** 613
[42] Heinrich G, Ludwig M, Qian J, Kubala B and Marquardt F 2011 *Phys. Rev. Lett.* **107** 043603
[43] Holmes C A, Meaney C P and Milburn G J 2012 *Phys. Rev.* E **85** 066203
[44] Giorgi G L, Galve F, Manzano G, Colet P and Zambrini R 2012 *Phys. Rev.* A **85** 052101
[45] Zhang M, Wiederhecker G S, Manipatruni S, Barnard A, McEuen P and Lipson M 2012 *Phys. Rev. Lett.* **109** 233906

[46] Bagheri M, Poot M, Fan L, Marquardt F and Tang H X 2013 *Phys. Rev. Lett.* **111** 213902
[47] Ludwig M and Marquardt F 2013 *Phys. Rev. Lett.* **111** 073603
[48] Hriscu A M and Nazarov Y V 2013 *Phys. Rev. Lett.* **110** 097002
[49] Mari A, Farace A, Didier N, Giovannetti V and Fazio R 2013 *Phys. Rev. Lett.* **111** 103605
[50] Lee T E and Sadeghpour H R 2013 *Phys. Rev. Lett.* **111** 234101
[51] Walter S, Nunnenkamp A and Bruder C 2014 *Phys. Rev. Lett.* **112** 094102
[52] Lee T E, Chan C K and Wang S 2014 *Phys. Rev.* E **89** 022913
[53] Walter S, Nunnenkamp A and Bruder C 2014 *Ann. Phys.* **527** 131
[54] Xu M, Tieri D A, Fine E C, Thompson J K and Holland M J 2014 *Phys. Rev. Lett.* **113** 154101
[55] Hermoso de Mendoza I, Pachón L A, Gómez-Gardeñes J and Zueco D 2014 *Phys. Rev.* E **90** 052904
[56] Ameri V, Eghbali-Arani M, Mari A, Farace A, Kheirandish F, Giovannetti V and Fazio R 2015 *Phys. Rev.* A **91** 012301
[57] Shlomi K, Yuvaraj D, Baskin I, Suchoi O, Winik R and Buks E 2015 *Phys. Rev.* E **91** 032910
[58] Zhang M, Shah S, Cardenas J and Lipson M 2015 *Phys. Rev. Lett.* **115** 163902
[59] Lauter R, Brendel C, Habraken S J M and Marquardt F 2015 *Phys. Rev.* E **92** 012902
[60] Hush M R, Li W, Genway S, Lesanovsky I and Armour A D 2015 *Phys. Rev.* A **91** 061401
[61] Weiss T, Kronwald A and Marquardt F 2016 *New J. Phys.* **18** 013043
[62] Lörch N, Amitai E, Nunnenkamp A and Bruder C 2016 *Phys. Rev. Lett.* **117** 073601
[63] Weiss T, Walter S and Marquardt F 2017 *Phys. Rev.* A **95** 041802(R)
[64] Kurths J, Pikovsky A and Rosenblum M 2001 *Synchronization: A Universal Concept in Nonlinear Sciences* (Cambridge: Cambridge University Press)